CLINICAL INVESTIGATIVE STUDY

JOURNAL OF
NEUROIMAGING
THE OFFICIAL JOURNAL OF THE AMERICAN SOCIETY OF NEUROIMAGING

WILEY

Brain ^{18}F-FDG-PET and an optimized cingulate island ratio to differentiate Lewy body dementia and Alzheimer's disease

Katharina Woyk[1] | Carsten Oliver Sahlmann[1] | Niels Hansen[2] | Charles Timäus[2] |
Sebastian Johannes Müller[3] | Eya Khadhraoui[3] | Jens Wiltfang[2,4,5] | Claudia Lange[2] |
Caroline Bouter[1]

[1]Department of Nuclear Medicine, University Medical Center Göttingen (UMG), Georg-August-University, Göttingen, Germany

[2]Department of Psychiatry and Psychotherapy, University Medical Center Göttingen (UMG), Georg-August-University, Göttingen, Germany

[3]Department of Neuroradiology, University Medical Center Göttingen (UMG), Georg-August-University, Göttingen, Germany

[4]Neurosciences and Signaling Group, Department of Medical Sciences, Institute of Biomedicine, University of Aveiro, Aveiro, Portugal

[5]German Center for Neurodegenerative Diseases, Göttingen, Germany

Correspondence
Caroline Bouter, Department of Nuclear Medicine, University Medical Center Göttingen (UMG), Georg-August-University, Robert Koch Str. 40, 37075 Göttingen, Germany.
Email: caroline.bouter@med.uni-goettingen.de

Abstract

Background and Purpose: The diagnosis of Dementia with Lewy Bodies (DLB) is challenging due to various clinical presentations and clinical and neuropathological features that overlap with Alzheimer's disease (AD). The use of ^{18}F-Fluorodeoxyglucose-PET (^{18}F-FDG-PET) can be limited due to similar patterns in DLB and AD. However, metabolism in the posterior cingulate cortex is known to be relatively preserved in DLB and visual assessment of the "cingulate island sign" became a helpful tool in the analysis of 18F-FDG-PET. The aim of this study was the evaluation of visual and semiquantitative 18F-FDG-PET analyses in the diagnosis of DLB and the differentiation to AD as well as its relation to other dementia biomarkers.

Methods: This retrospective study comprises 81 patients with a clinical diagnosis of DLB or AD that underwent ^{18}F-FDG-PET/CT. PET scans were analyzed visually and semiquantitatively and results were compared to clinical data, cerebrospinal fluid results, dopamine transporter scintigraphy, and 18F-Florbetaben-PET. Furthermore, different cingulate island ratios were calculated to analyze their diagnostic accuracy.

Results: Visual assessment of 18F-FDG-PET showed an accuracy of 62%-77% in differentiating between DLB and AD. Standard uptake values were significantly lower in the primary visual cortex and the lateral occipital cortex of DLB patients compared to AD patients. The cingulate island ratio was significantly higher in the DLB group compared to the AD group and the ratio posterior cingulate cortex to visual cortex plus lateral occipital cortex showed the highest diagnostic accuracy to discriminate between DLB and AD at 81%.

Conclusions: Semiquantitative 18F-FDG-PET imaging and especially the use of an optimized cingulate island ratio are valuable tools to differentiate between DLB and AD.

KEYWORDS
^{18}F-FDG-PET, cingulate island sign, Alzheimer's disease, Dementia with Lewy Bodies

INTRODUCTION

Advanced age has been identified as a significant risk factor for the development of dementia. Consequently, as life expectancy of the world's population increases, the significance of dementia is constantly growing. The global prevalence of dementia is expected to increase by approximately 2.7-fold by 2050.[1] Following Alzheimer's dementia (AD), Dementia with Lewy Bodies (DLB) is the second most common form of dementia with a prevalence of about 5% in the elderly population and an expected high number of misdiagnosed cases, especially in early stages of the disease.[2]

DLB is characterized by an abnormal intraneuronal aggregation of α-synuclein leading to the formation of Lewy bodies and Lewy neurites. Clinically, DLB is characterized as a progressive cognitive decline with four accompanying core symptoms: fluctuating cognition, recurrent visual hallucinations, rapid eye movement (REM) sleep behavior disorder, and parkinsonism.[3] However, the appearance and combination of these symptoms largely vary in DLB patients as well as their initial clinical presentation. Based on initial symptoms, three clinical prodromal DLB subtypes were proposed including mild cognitive impairment (MCI) onset, psychiatric onset, and delirium onset.[4] Furthermore, clinical presentations and pathological features can overlap with AD complicating the diagnosis.[5] Therefore, the diagnosis of DLB remains a major challenge, especially in early stages of the disease.

In 2017, the fourth consensus report of the DLB consortium defined clinical features and diagnostic biomarkers for an improved diagnosis of DLB. Biomarkers were classified into indicative (including dopamine transporter imaging, [superscript]123[/superscript]Iodine-metaiodobenzylguanidine myocardial imaging [[superscript]123[/superscript]I-MIBG] myocardial scintigraphy, and polysomnographic confirmation of REM sleep disorder) and supportive biomarkers (including CT or MRI, brain perfusion scintigraphy or [superscript]18[/superscript]F-fluorodeoxyglucose [[superscript]18[/superscript]F-FDG]-PET, and specific electroencephalogram abnormalities).

The common imaging biomarker [superscript]18[/superscript]F-FDG-PET was only considered as a supportive biomarker as the diagnostic accuracy in the differentiation to AD has been shown below the critical cutoff of 80% for a valid biomarker.[3,6] Visual [superscript]18[/superscript]F-FDG-PET interpretation can be hampered as AD and DLB can show similar patterns with prefrontal, posterotemporal, and parietal hypometabolism. While DLB patients usually show a more severe hypometabolism in the occipital cortical areas, preserved occipital metabolism in DLB patients can further complicate the differentiation to AD.

Furthermore, the so-called "cingulate island sign" can be used for the differentiation between DLB and AD as AD patients show a severe hypometabolism of the posterior cingulate at an early stage, while DLB patients show a relatively preserved metabolism of the posterior cingulate cortex compared to the reduced metabolism of surrounding cortical areas. On visual interpretation, the cingulate island sign achieved a high specificity in the diagnosis of DLB up to 100% with lower sensitivities of 73%-77%.[7,8]

Semiquantitative interpretation of [superscript]18[/superscript]F-FDG-PET scans can provide a useful add-on to the visual interpretation elaborating more subtle differences in different cortical areas. The use of statistical mapping has been well implemented into the clinical assessment of PET scans. However, the role of semiquantitative interpretation of [superscript]18[/superscript]F-FDG-PET and the use of cutoffs in the diagnosis of DLB remain unclear, especially in its differentiation to AD.

The aim of this study was the evaluation of [superscript]18[/superscript]F-FDG-PET imaging in a clinical cohort of DLB patients using different semiquantitative approaches for the differentiation of DLB and AD patients and its relation to other dementia biomarkers.

METHODS

Patient population

All patients with a clinical diagnosis of DLB or AD according to clinical criteria proposed by McKeith et al.[3] and Dubois et al.[9] who underwent [superscript]18[/superscript]F-FDG-PET/CT in our facility and presented between 2013 and 2021 were included in this retrospective study. Clinical diagnosis was established on the basis of clinical data and the patient's medical records. Only patients with a diagnosis of "probable DLB" or "possible DLB" according to the McKeith criteria and patients with a diagnosis of "highly probable AD" or "probable AD" according to the Dubois criteria for the likelihood of AD were included.[3,9] Patient characteristics, cerebrospinal fluid (CSF) biomarkers, Mini Mental State Examination (MMSE), and [superscript]18[/superscript]F-FDG-PET were assessed. If available, results of dopamine transporter SPECT with [superscript]123[/superscript]I-fluoropropyl carbomethoxyiodophenyl nortropane ([superscript]123[/superscript]I-FP-CIT; DaTSCAN®) and [superscript]18[/superscript]F-Florbetaben-PET ([superscript]18[/superscript]F-FBB-PET) were also included.

All procedures were in accordance with the ethical standards of the institutional and/or national research committee and with the 1964 Helsinki declaration and its later amendments or comparable ethical standards. The institutional review board approved this retrospective study. All patients signed an informed consent.

[superscript]18[/superscript]F-Fluorodeoxyglucose-PET/CT

All scans were acquired using a Philips Vereos PET/CT scanner (Philips Medical Systems, Cleveland, OH, USA) with a 128 × 128 matrix and a slice thickness of 2 mm. Images were acquired 60 minutes after the intravenous injection of a mean activity of 206 MBq (±35 MBq)[superscript]18[/superscript]F-FDG with a scan duration of 10 minutes. All images were reconstructed using an ordered subset-expectation maximization (OSEM) algorithm with three reconstruction iterations and 15 subsets. A low-dose CT scan was used for attenuation correction (CTAC-SG algorithm). All patients fasted at least 6 hours prior to the tracer injection. Blood sugar levels were measured in order to exclude for hyperglycemia (blood glucose >150 mg/dl). All patients rested for 20 minutes in a quiet and dimmed room prior to and for 10 minutes after tracer injection.

PET images were spatially normalized, processed, and co-registered automatically to a standard MRI template (ICBM152 Atlas, Montreal
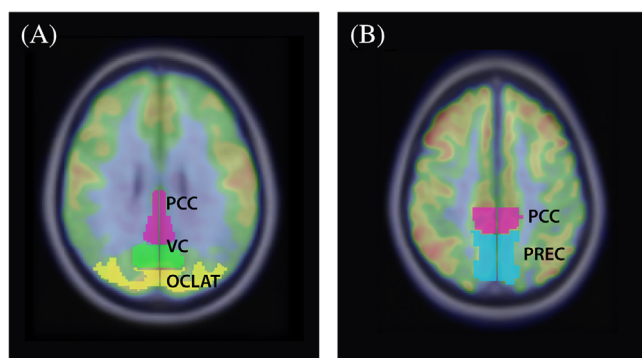
FIGURE 1 Volumes of interest (VOI) for the definition of different cingulate island ratios. (A, B) Fused 18F-FDG-PET/MRI images in axial plane. VOI definition was based on an MRI template. OCLAT, lateral occipital cortex (yellow); PCC, posterior cingulate cortex (magenta); PREC, precuneus (blue); VC, visual cortex (green)

Neurological Institute/International Consortium for Brain Mapping) using the CortexID® software (GE Healthcare, Chicago, IL, USA) as described before.[10,11] Volumes of interest (VOIs) were defined in 14 cortical regions according to an MRI-based brain atlas including lateral prefrontal cortex, medial prefrontal cortex, sensorimotor cortex, anterior cingulate cortex, posterior cingulate cortex, precuneus, superior parietal cortex, inferior parietal cortex, lateral temporal cortex, mesial temporal cortex, primary visual cortex, lateral occipital cortex, pons, and cerebellum. The pons region was used for image normalization. After preprocessing, images underwent a voxel-wise, single-subject statistical analysis with a comparison to healthy sex- and age-matched controls provided by the CortexID software with an output of individual patients' VOI z-scores and z-score maps presented as 3-dimensional Stereotactic Surface Projection (3D-SSP) images of the cortex with a threshold of 2 standard deviations (SD). The Cortex ID normal database contains more than 100 subjects with no memory or other cognitive complaints and no evidence of neurodegenerative diseases aged 42-89. The normal database was stratified into five age groups: <60, 60-70, 71-90, ≥80, and all ages. PET analysis was performed by 2 individual experienced readers who were blinded for the patient's history and diagnosis. Randomly presented PET scans and 3D-SSP maps were used for choosing a diagnosis as follows: (1) occipital hypometabolism (especially lateral occipital cortex and primary visual cortex) matching a typical DLB pattern; (2) hypometabolism in the posterior cingulate cortex, precuneus, and posterior temporal cortex matching a typical AD pattern; or (3) uncertain (unspecific or diffuse cortical hypometabolism).

Furthermore, the presence of significant lateral and medial hypometabolism was assessed using a 2-SD threshold and was considered positive if z-scores were >2 SD within medial and lateral cortical areas as postulated before.[12]

The "cingulate island ratio" was defined as the standard uptake values (SUV) within the VOI of the posterior cingulate cortex (PCC) divided by the SUV in the precuneus (PREC) plus primary visual cortex region (VC; Figure 1) and further ratios were defined as described below.

18F-Florbetaben PET/CT

Amyloid PET was performed with 18F-FBB (Life Molecular Imaging GmbH, Berlin, Germany; mean activity 315 ± 14 MBq). Image acquisition was started 90 minutes (min) postinjection with an acquisition time of 20 minutes according to the manufacturer's protocol. Acquisition parameters and image reconstruction was performed as described above.

18F-FBB-PET scans were evaluated by an experienced specialist that underwent a specific reader training for 18F-FBB-PET imaging. Scans were visually scored "negative" if the tracer uptake was limited to the physiological unspecific white matter uptake with a clear gray/white matter contrast and scored "positive" if tracer uptake in the gray matter was increased in at least two cortical areas loosing gray/white matter contrast. Amyloid uptake was also assed semi-quantitatively using the CortexID® software. In brief, automated gray matter segmentation was performed after anatomic normalization using a T1-weighted MRI-template and nine reference regions were defined (frontal cortex, anterior and posterior cingulate cortex, mesial and lateral temporal cortex, parietal cortex, occipital cortex, whole cortex, and cerebellar cortex). Standardized uptake values of these regional volumes were obtained and standardized uptake value ratios were calculated using the whole cerebellum as reference region.

Cerebrospinal fluid

ß-Amyloid 42 (Aß42) and ß-amyloid 40 (Aß40) were measured in the Neurochemistry Laboratory of the University Medical Center Göttingen using commercially available INNOTEST® β-AMYLOID (1-42) ELISA kit (Fujirebio) and ELISA from IBL (AMYLOID BETA [1-40]). The ratio Aß42/40 was calculated and considered as pathological if values were <.5. Aß42 values were considered pathological if <450 pg/ml. Values of total tau (t-tau) were considered pathological if >450 pg/ml and of phosphorylated tau (p-tau) if >61 pg/ml.

Statistical analysis

Statistical analysis was performed using SPSS Statistics version 27 (IBM, Armonk, NY, USA) and GraphPad Prism version 9 (GraphPad Software, San Diego, CA, USA).

Differences between groups were tested using unpaired t-test or univariate analysis of variance (ANOVA) for continuous variables and Chi-square test for categorical variables as indicated. Univariate analysis of covariance (ANCOVA) was used for covariate adjustment as indicated. Receiver-operating characteristic analysis was used for the evaluation of the accuracy of the diagnostic tests. Relationships between variables were assessed using Pearson's correlation and simple linear regression. Interrater agreement was quantified by Kappa results using GraphPad Quickcals (https://www.graphpad.com/quickcalcs/kappa2/).

TABLE 1 Patient characteristics

	DLB (n = 36)	AD (n = 45)	p-value
Age (years)	77.68 ± 8.6	70.44 ± 10.6	.0004
MMSE	23.72 ± 4.9	22.0 ± 5.1	.1703
Sex			.1913
Female (n)	15	25	
Male (n)	21	20	

Note: All the data represent mean ± standard deviation unless otherwise indicated.
Abbreviations: AD, Alzheimer's dementia; DLB, Dementia with Lewy Bodies; MMSE, Mini Mental State Examination; *n*, number of subjects.

Data are given as mean ± SD. Significance levels are given as follows: *p < .05, **p < .01, and ***p < .0001.

RESULTS

Patient characteristics

A total of 36 DLB and 45 AD patients were included in this study. Baseline characteristics are shown in Table 1. The group of DLB patients was significantly older compared to the AD group (*p* = .0039; unpaired *t*-test). MMSE did not show significant differences between DLB and AD patients (*p* = .1703; unpaired *t*-test), neither did the gender distribution (*p* = .2742; Chi-square test).

The diagnosis of DLB or AD was determined by clinical criteria as proposed by McKeith et al.[3] and Dubois et al.[9]

In the DLB group, 28 patients were diagnosed as "probable DLB" showing two or more core clinical features or the combination of one core clinical feature and one indicative biomarker (Table 2). Eight patients were diagnosed as "possible DLB" according to the McKeith criteria showing one core clinical features or one or more indicative biomarkers. In the AD group, no patient showed any core clinical features for DLB. Eighteen patients of the AD group showed symptoms of depression. All other patients of the AD group did not show any supportive clinical features or indicative biomarkers for a DLB diagnosis according to the McKeith criteria.

In the AD group, 41 patients were diagnosed as "highly probable AD" and 4 as "probable AD" according to the Dubois criteria for the likelihood of AD as a primary diagnosis (Table 3). Twenty-nine patients showed mainly amnestic symptoms, while 5 patients presented with aphasic symptoms and 11 patients showed both amnestic and aphasic symptoms. All 41 "highly probable AD" cases were amyloid and tau positive (positive Aβ42 and/or Aβ42/40 ratio in CSF: *n* = 18; positive amyloid PET: *n* = 15; positive PET and CSF: *n* = 7; positive t-tau or p-tau in CSF: *n* = 41). Mean CSF Aβ42 was 556.9 ± 129.8 pg/ml and mean Aβ42/40 ratio was .42 ± .079. Mean t-tau was 766.4 ± 402.4 pg/ml and mean p-tau was 98.57 ± 33.48 pg/ml (Table 4). All 4 patients diagnosed as "probable AD" according to the Dubois criteria were amyloid positive (positive Aβ42 and/or Aβ42/40 ratio in CSF: *n* = 2; positive amyloid

TABLE 2 DLB diagnosis according to McKeith criteria

	Probable DLB (n = 28)	Possible DLB (n = 8)	AD (n = 45)
Core clinical features			
Fluctuating cognition (n)	10	-	-
Recurrent visual hallucinations (n)	14	1	-
Parkinsonism (n)	21	6	-
Supportive clinical features			
Hallucinations in other modalities (n)	1	2	-
Depression (n)	17	1	18
Systematized delusions (n)	9	2	-
Hyposmia (n)	1		
Hypersomnia (n)	2	-	
Anxiety (n)	2	-	
Severe sensitivity to antipsychotic agents (n)	1	-	
Apathy (n)	1	-	
Indicative biomarkers			
Positive ^{123}I-FP-CIT scan (n)	24 (of 25)	3 (of 6)	0 (of 4)
Supportive biomarkers			
Typical DLB pattern in FDG-PET (n; reader 1/reader2)	23/18	5/5	5/4

Abbreviations: AD, Alzheimer's dementia; DLB, Dementia with Lewy Bodies; ^{123}I-FP-CIT, ^{123}I-fluoropropyl carbomethoxyiodophenyl nortropane; *n*, number of subjects.

TABLE 3 AD patients according to Dubois criteria

	Highly probable AD (n = 41)	Probable AD (n = 4)
Clinical phenotype		
Amnestic symptoms (n)	25	2
Aphasic symptoms (n)	4	1
Both (n)	12	1
Biomarker		
Amyloid positive (n)	41	4
Tau-positive (n)	41	-

Abbreviations: AD, Alzheimer's dementia; *n*, number of subjects.

PET: *n* = 1; positive PET and CSF: *n* = 1) and tau negative. Mean Aβ42 was 621.5 ± 164.3 pg/ml and mean Aβ42/40 ratio was .61 ± .117. Mean t-tau was 403.3 ± 45.02 pg/ml and mean p-tau was 50.0 ± 5.83 pg/ml.

Aβ42 and t-tau did not show significant differences between "highly probable AD" and "probable AD" patients (Aβ42: *p* = .3986; t-tau: *p* = .0823; unpaired *t*-test), while Aβ42/40 was significantly lower in the "highly probable AD" group (*p* = .008; unpaired *t*-test) and p-tau

WILEY

TABLE 4 CSF and PET biomarkers in AD and DLB patients

	Highly probable AD (n = 41)	Probable AD (n = 4)	DLB (n = 36)	p-value; ANCOVA
CSF biomarkers				
Aβ42 (pg/ml)	556.9 (130)	621.5 (164)	868 (319)	.001
Aβ42/40 ratio (pg/ml)	0.4222 (0.08)	0.6075 $\pm$ 0.12	0.8859 (0.38)	<.0001
t-tau (pg/ml)	766.6 $\pm$ 402.4	403.3 $\pm$ 45.02	379.9 (207)	<.0001
p-tau (pg/ml)	98.57 $\pm$ 33.48	50.0 $\pm$ 5.83	57.43 (27)	<.0001
PET biomarkers				
Positive amyloid PET (n)	23 (of 23)	2 (of 2)	5 (of 8)	

Note: All the data represent mean $\pm$ standard deviation unless otherwise indicated.
Abbreviations: AD, Alzheimer's dementia; ANCOVA, univariate analysis of covariance; DLB, Dementia with Lewy Bodies; n, number of subjects.

was significantly higher in the "highly probable AD" group (p = .0067; unpaired t-test).

18F-FDG-PET results

Visual assessment

18F-FDG-PET was available in all patients. In the DLB group, reader 1 rated n = 29 as "typical DLB pattern," n = 4 as "AD pattern," and n = 3 as "uncertain." Reader 2 rated n = 23 as "typical DLB pattern," n = 2 as "AD pattern," and n = 11 as "uncertain."

For the AD group, reader 1 rated n = 33 as "typical AD pattern," n = 5 as "DLB pattern," and n = 7 as "uncertain." Reader 2 rated n = 27 as "typical AD pattern," n = 4 as "DLB pattern," and n = 14 as "uncertain" (Figure 2).

Interreader agreement showed a "substantial agreement" with a kappa of .644 (standard error [SE] of kappa = .066; 95% confidence interval [CI] from .515 to .773). The sensitivity of a visual DLB diagnosis in 18F-FDG-PET was 64%-80% and the specificity was 60%-73% with an accuracy of 62%-77%. The sensitivity of a visual AD diagnosis in 18F-FDG-PET was 60%-73% with a specificity of 85% and an accuracy of 69%-79%.

Semiquantitative assessment

18F-FDG uptake was quantitatively analyzed using SUVs in different cortical regions. SUV negatively correlated with age in several brain regions in both the DLB and the AD group and gender differences were seen in a few single brain regions. Therefore, 18F-FDG-PET data were adjusted to age and gender as covariates.

DLB versus AD

SUV was significantly lower in the primary visual cortex ($p \leq$ .0001) and the lateral occipital cortex (p = .026) of DLB patients compared to AD patients after adjusting for age and gender as covariates (ANCOVA; Figure 3A).

All other brain regions did not show significant differences between of the SUV the DLB and AD groups (prefrontal lateral cortex: p = .664; prefrontal medial cortex: p = .945; sensorimotor cortex: p = .266; anterior cingulate cortex: p = .874; posterior cingulate cortex: p = .174; precuneus: p = .945; superior parietal cortex: p = .539; inferior parietal cortex: p = .698; lateral temporal cortex: p = .65; mesial temporal cortex: p = .652; cerebellum: p = .562; ANCOVA; Figure 3A).

The primary visual cortex showed a higher accuracy for differentiating DLB from AD (area under the curve [AUC] = .7648; 95% CI: .6594 to .8703; Figure 3B) compared to the lateral occipital cortex (AUC = .6599; 95% CI: .5391 to .7807; Figures 3B and 4). The optimal cutoff SUV in the primary visual cortex score to discriminate between DLB and AD was <1.348 (sensitivity: 63.89%; specificity: 80.0%) and <1.273 for the lateral occipital cortex (sensitivity 61.11%; specificity 68.89%).
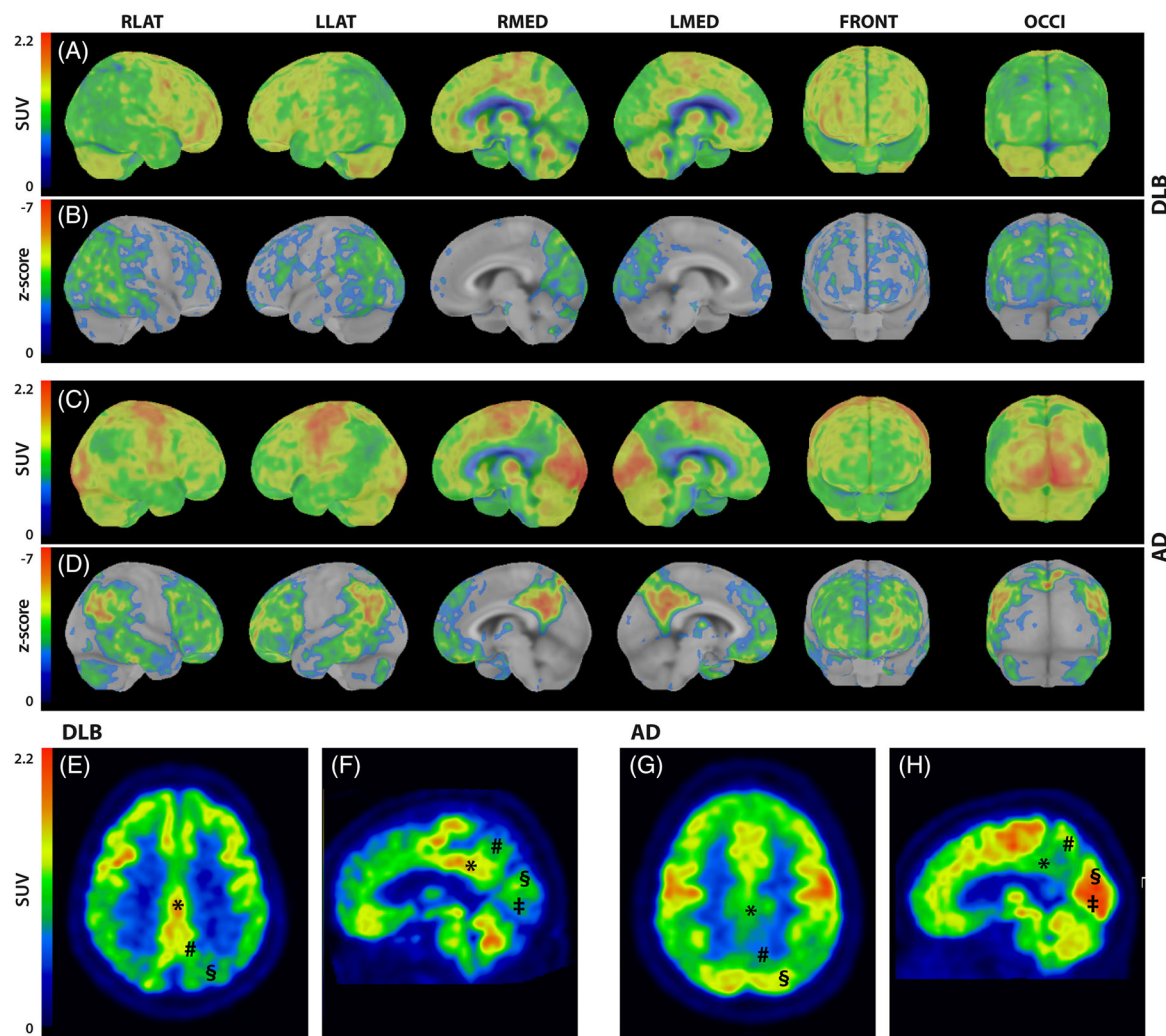
Occipital hypometabolism

As described before, occipital hypometabolism showed a high discriminative ability in the diagnosis of DLB. Therefore, we analyzed the presence of occipital hypometabolism in the DLB and the AD group defined as medial and lateral occipital hypometabolism with z-scores >–2 SD compared to the normal cohort. Twenty-six patients (72%) met the criteria for occipital hypometabolism in the DLB group and 18 patients in the AD group (40%).

Cingulate island sign

A cingulate island sign was visually detected in 23 DLB cases by reader 1 and in 21 DLB cases by reader 2 (Figure 2E-H) as well as in 0 AD cases by reader 1 and in 3 AD cases by reader 2. The interrater agreement of the visual cingulate island sign showed a "substantial agreement" with a kappa of .795 (SE of kappa = .097; 95% CI from .605 to .986). The

FIGURE 2 ^{18}F-FDG-PET. (A-D) Surface projection and z-score maps of 18F-FDG-PET. (A) Representative ^{18}F-FDG-PET of a DLB patient with distinct hypometabolism in the lateral and medial occipital cortex, temporoparietal cortex, and lateral frontal cortex. (B) Corresponding Z-score maps of the DLB patient with a threshold of −2 standard deviations compared to a normal cohort. (C) Representative ^{18}F-FDG-PET of an AD patient with distinct hypometabolism in the temporoparietal cortex, posterior cingulate cortex, precuneus, and lateral and medial frontal cortex. (D) Corresponding Z-score maps of the AD patient with a threshold of −2 standard deviations compared to a normal cohort. (E-H) Cingulate island sign. (E-F) ^{18}F-FDG-PET of a DLB patient in axial (E) and sagittal (F) plane with a severe hypometabolism in the precuneus, visual cortex, and occipital lateral cortex, while ^{18}F-FDG uptake is relatively preserved in the posterior cingulate cortex. (G, H) ^{18}F-FDG-PET of an AD patient in axial (G) and sagittal (H) plane with a severe hypometabolism in the posterior cingulate cortex, while ^{18}F-FDG uptake in the visual cortex and occipital lateral cortex is relatively preserved. AD, Alzheimer's disease; DLB, Dementia with Lewy Bodies; OCLAT, lateral occipital cortex; PCC, posterior cingulate cortex; PREC, precuneus; SUV, standard uptake value; VC, visual cortex; RLAT, right lateral view; LLAT, left lateral view; RMED, right medial view; LMED, left medial view; FRONT, frontal view; OCCI, occipital view

sensitivity of visual cingulate island sign assessment was 58%-64% and the specificity was 93%-100%.

In order to quantitatively assess the cingulate island sign, the cingulate island ratio was calculated as previously described in the literature (PCC/(PREC+VC); Figure 5).[7] The cingulate island ratio PCC/(PREC+VC) was significantly higher in DLB patients compared to AD patients adjusted for age and gender as covariates ($p < .001$; ANCOVA; Figure 5). The optimal cutoff score for the cingulate island ratio to discriminate between DLB and AD was >.4995 with a sensitivity of 61.11% and specificity of 71.1% (AUC = .7716; 95% CI: .6722 to .8710).

Other cingulate island ratios

Different ratios that represent the visual aspect of the cingulate island sign were formed in order to analyze their diagnostic accuracy compared to the commonly used cingulate island ratio PCC/(PREC+VC).

The ratio PCC/(VC+ lateral occipital cortex [OCLAT]) showed the highest diagnostic accuracy to discriminate between DLB and AD with an optimal cutoff score >.5103 with a specificity of 82.22% and a sensitivity of 75% (AUC = .8136; 95% CI: .7205 to .9066; Figure 4). Therefore, the cingulate island ratio PCC/(VC+OCLAT) was
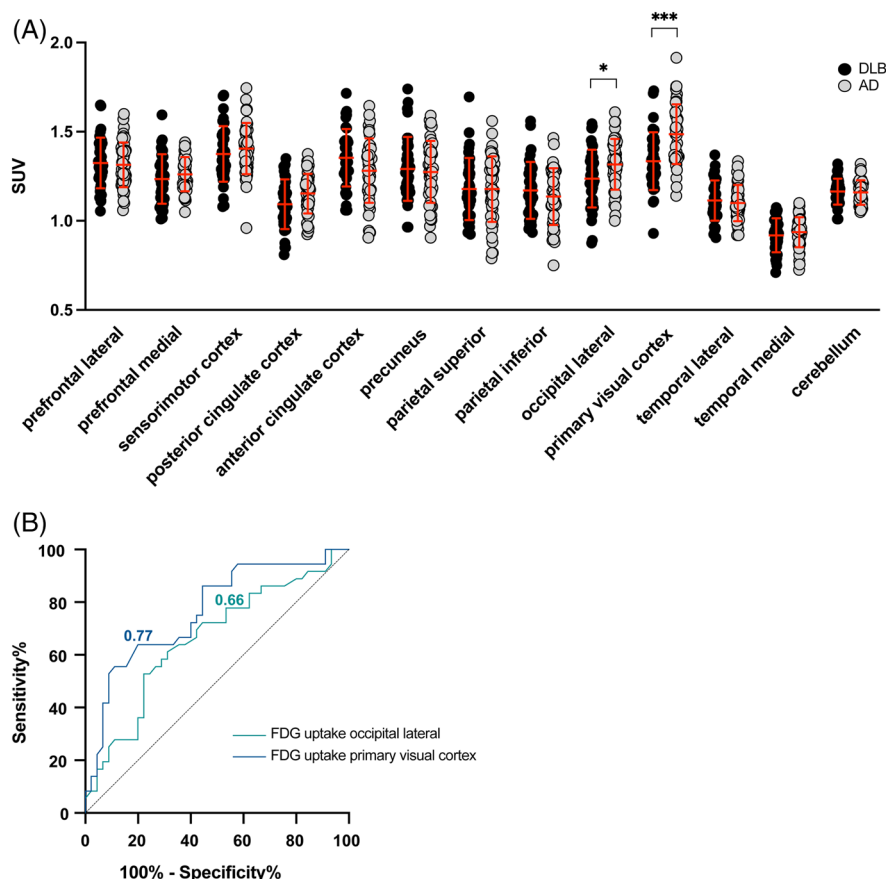
FIGURE 3 FDG-PET quantification. (A) SUV was significantly lower in DLB patients in the primary visual cortex and the lateral occipital cortex. All other brain regions did not show significant differences. Univariate analysis of covariance; *$p < .05$; ***$p < .0001$. (B) Receiver-operating characteristic analysis. Diagnostic accuracy for differentiating DLB from AD was higher in the primary visual cortex compared to the lateral occipital cortex. The dotted line shows the diagonal reference. AD, Alzheimer's dementia; DLB, Dementia with Lewy Bodies; FDG, fluorodeoxyglucose; SUV, standard uptake value

considered as the best ratio representing a cingulate island sign and was used for further analysis in this study.

DLB onset

DLB patients were categorized according to the onset of the disease (delirium onset, MCI onset, or psychiatric onset; according to McKeith et al.[22]). Nineteen patients showed a psychiatric onset including depression, anxiety, or delusions, 11 patients showed an MCI onset, and 6 patients showed a mixed onset with concurrently onset of psychiatric and MCI symptoms. No patients with a delirium onset were found within our cohort.

18F-FDG-PET scans were acquired 5-170 months (mean: 55 months) after the patients have noticed first symptoms. 18F-FDG uptake of mixed-onset patients was significantly lower compared to MCI-onset patients in the lateral prefrontal cortex ($p = .006$), precuneus ($p = .034$), inferior parietal cortex ($p = .015$), and lateral temporal cortex ($p = .014$; ANCOVA and Bonferroni pairwise comparison test; Figure 6) while adjusted for age and gender as covariates. 18F-FDG uptake was significantly lower in the posterior cingulate

cortex ($p = .044$), precuneus ($p = .049$), and lateral temporal cortex ($p = .036$; ANCOVA and Bonferroni pairwise comparison test; Figure 6) of mixed-onset patients compared to psychiatric onset patients while adjusted for age and gender. SUV did not show significant differences between the three onset groups in the other cerebral regions (medial prefrontal cortex: $p = .062$; sensorimotor cortex: $p = .316$; anterior cingulate cortex: $p = .879$; superior parietal cortex: $p = .074$; lateral occipital cortex: $p = .063$; primary visual cortex: $p = .097$; mesial temporal cortex: $p = .993$; cerebellum: $p = .162$; ANCOVA; Figure 6).

The cingulate island ratio PCC/(VC+OCLAT) did not show significant differences between the different onset groups ($p = .337$; ANCOVA and Bonferroni pairwise comparison test).

Other biomarkers

Amyloid PET

18F-FBB-PET was available in 8 DLB and 25 AD patients. Four DLB patients and 25 AD patients showed a pathological 18F-FBB-uptake.
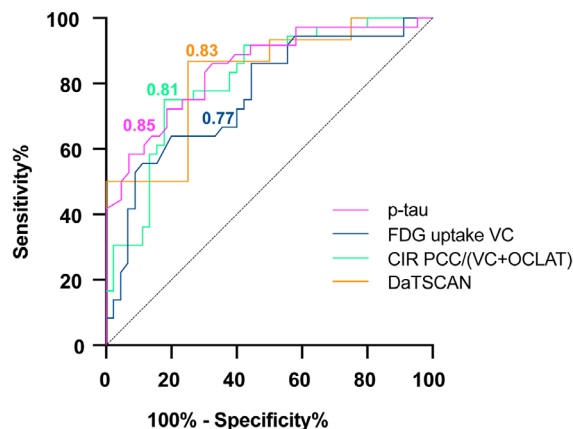
FIGURE 4 Diagnostic accuracy of imaging and CSF biomarkers in the differentiation between DLB and AD. Receiver-operating characteristic analysis. p-tau showed the highest accuracy in differentiating DLB from AD followed by 123I-FP-CIT scintigraphy, and the cingulate island ratio PCC/(VC+OCLAT). The dotted line shows the diagonal reference. CIR, cingulate island ratio; FDG, fluorodeoxyglucose; 123I-FP-CIT, 123I-fluoropropyl carbomethoxyiodophenyl nortropane; OCLAT, lateral occipital cortex; PCC, posterior cingulate cortex; SUV, standard uptake value; VC, primary visual cortex

Whole cortex SUV did not show significant differences between amyloid PET-positive patients in the AD group compared to the DLB group while adjusted for age and gender as covariates ($p = .062$; ANCOVA; Figure 7A).

There was no correlation between ^{18}F-FBB and ^{18}F-FDG uptake, neither in the DLB nor in the AD group ($p > .09$ in all brain areas; Pearson's correlation). There was no significant correlation between the cingulate island ratio PCC/(VC+OCLAT) and ^{18}F-FBB uptake in both groups (DLB: $p = .0598$; $r = .687$; AD: $p = .3697$; $r = -.201$; Pearson's correlation).

Dopamine transporter scintigraphy with ^{123}I-FP-CIT

^{123}I-FP-CIT scintigraphy was available in 32 DLB and 4 AD patients. Twenty-six DLB patients showed abnormal scans. Remaining DLB patients ($n = 6$) and all AD cases ($n = 4$) showed a physiological tracer uptake. Striatal uptake was significantly lower in DLB patients compared to AD patients ($p = .0361$; ANOVA) with high diagnostic accuracy in the differentiation between DLB and AD (AUC = .825; 95% CI: .6156 to 1; Figure 4). The tracer uptake did not correlate with amyloid load in ^{18}F-FBB-PET or with cortical 18-F-FDG uptake ($p > .54$ in all areas; Pearson correlation). Different DLB onset subtypes did not show significant differences ($p = .1232$; ANOVA).

CSF biomarkers

CSF biomarkers Aβ42, Aβ42/40 ratio, t-tau, and p-tau were available in all DLB patients and in $n = 43$ AD patients. Aβ42 and the Aβ42/40 ratio were significantly higher in DLB patients compared to AD patients while adjusted for age and gender as covariates (Aβ42: $p = .001$; Aβ42/40 ratio: $p < .0001$; ANCOVA; Figure 7C,D).

Both t-tau and p-tau were significantly lower in the DLB group compared to AD ($p < .0001$; ANCOVA; Figure 7E,F). p-tau showed the highest accuracy in differentiating DLB from AD (AUC = .8472; 95% CI: .7612 to .9332) with an optimal cutoff value of <63.5 with a specificity of 86.05% and a sensitivity of 63.89% (Figure 7).

Different DLB onset groups did not show significant differences in CSF biomarkers (Aβ42: $p = .259$; Aβ42/40 ratio: $p = .157$; t-tau: $p = .262$; p-tau: $p = .173$; ANCOVA and Bonferroni pairwise comparison test).

Correlation between FDG-PET and CSF biomarkers

FDG uptake in DLB patients did not correlate with Aβ42 and the Aβ42/40 in CSF ($p > .17$ in all regions; Pearson's correlation). CSF t-tau did not correlate with FDG uptake in DLB patients except for the mesial temporal region ($p = .0326$, $r = -.3521$; all other regions $p > .15$; Pearson's correlation), neither did FDG uptake correlate with p-tau in CSF except for the superior parietal cortex ($p = .019$, $r = -.384$; all other regions $p > .065$; Pearson's correlation).

In AD patients, FDG uptake correlated with Aβ42 in several brain regions (Aβ42: lateral prefrontal cortex: $p = .0014$; $r = .4728$; medial prefrontal cortex: $p = .0024$; $r = .4516$; posterior cingulate cortex: $p = .0483$, $r = .303$; precuneus: $p = .00052$; $r = .4183$; superior parietal cortex: $p = .0245$; $r = .3426$; inferior parietal cortex: $p = .0023$, $r = .4525$; lateral occipital cortex: $p = .0017$; $r = .4655$; Pearson's correlation), while the Aβ42/40 ratio did not correlate with SUV ($p > .068$ in all regions; Pearson's correlation).

FDG uptake correlated with t-tau in the AD group in the lateral prefrontal ($p = .013$, $r = -.3756$), precuneus ($p = .0318$, $r = -.328$), and inferior parietal region ($p = .042$, $r = -.3116$; all other regions $p > .085$), while CSF p-tau did not correlate with FDG uptake ($p > .095$ in all regions; Pearson's correlation).

The cingulate island ratio PCC/(VC+OCLAT) did not correlate with CSF biomarkers Aβ42, Aβ42/40 ratio, p-tau, or t-tau neither in DLB nor in AD patients ($p > .2003$ in all regions; Pearson's correlation).

Mini Mental State Examination

MMSE did not show significant differences between DLB and AD patients ($p = .231$; unpaired t-test; Figure 7B). MMSE did not correlate with the cingulate island ratio PCC/(VC+OCLAT) neither in DLB nor in AD patients (DLB: $p = .3468$, $r = .16912$; AD: $p = .9707$, $r = -.0065$). There was no significant correlation between MMSE and CSF biomarkers Aβ42, Aβ42/40, t-tau, or p-tau in both groups (DLB: Aβ42: $p = .5979$, $r = .0969$; Aβ42/40: $p = .7186$, $r = -.0663$; t-tau: $p = .3892$, $r = .1575$; p-tau: $p = .2617$, $r = .2044$; AD: Aβ42: $p = .2023$, $r = .2439$, Aβ42/40: $p = .6966$, $r = .0756$, t-tau: $p = .8341$, $r = -.041$; p-tau: $p = .784$, $r = .0512$).
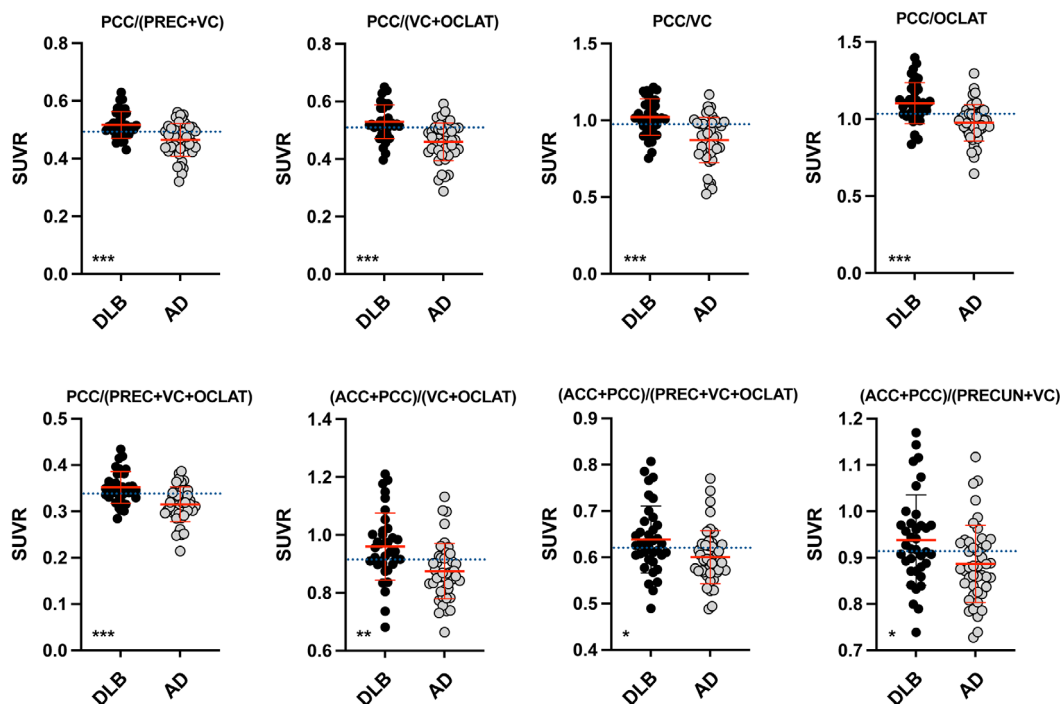
FIGURE 5   Cingulate island sign quantification. Different SUV ratios were formed in order to quantitatively characterize the cingulate island sign. All calculated ratios showed significant differences between the DLB and AD groups. Univariate analysis of covariance; $*p < .05$; $**p < .001$; $***p < .0001$. The blue dotted lines represent the optimal cutoff scores that were calculated by receiver-operating characteristic analysis. ACC, anterior cingulate cortex; AD, Alzheimer's dementia; DLB, Dementia with Lewy Bodies; OCLAT, lateral occipital cortex; PCC, posterior cingulate cortex; PREC, precuneus; SUVR, standard uptake value ratio; VC, primary visual cortex
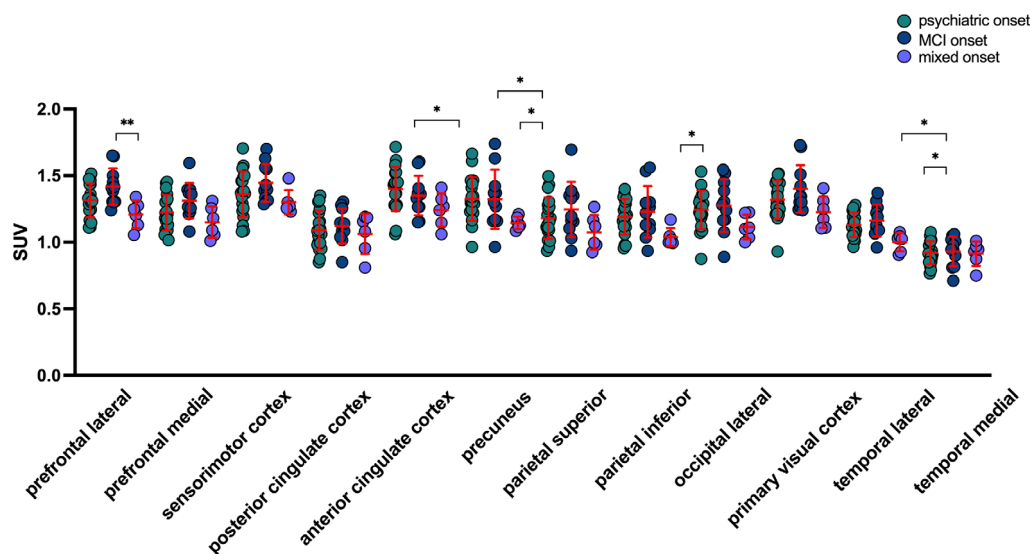

FIGURE 6   DLB onset. FDG uptake of mixed-onset patients was significantly lower in several cortical areas compared to psychiatric-onset and MCI-onset patients. Univariate analysis of covariance; $*p < .05$; $**p < .001$. MCI, mild cognitive impairment; FDG, fluorodeoxyglucose; SUV, standard uptake value

DISCUSSION

The clinical diagnosis of DLB remains a major challenge for both clinicians and molecular imaging experts. Studies on biomarkers for a reliable diagnosis of DLB have been controversial, with only a few biomarkers being significant enough for supporting a clinical suspicion of DLB.[13] Here, we assessed the performance of ^{18}F-FDG-PET in the diagnosis and differential diagnosis of DLB compared to AD.
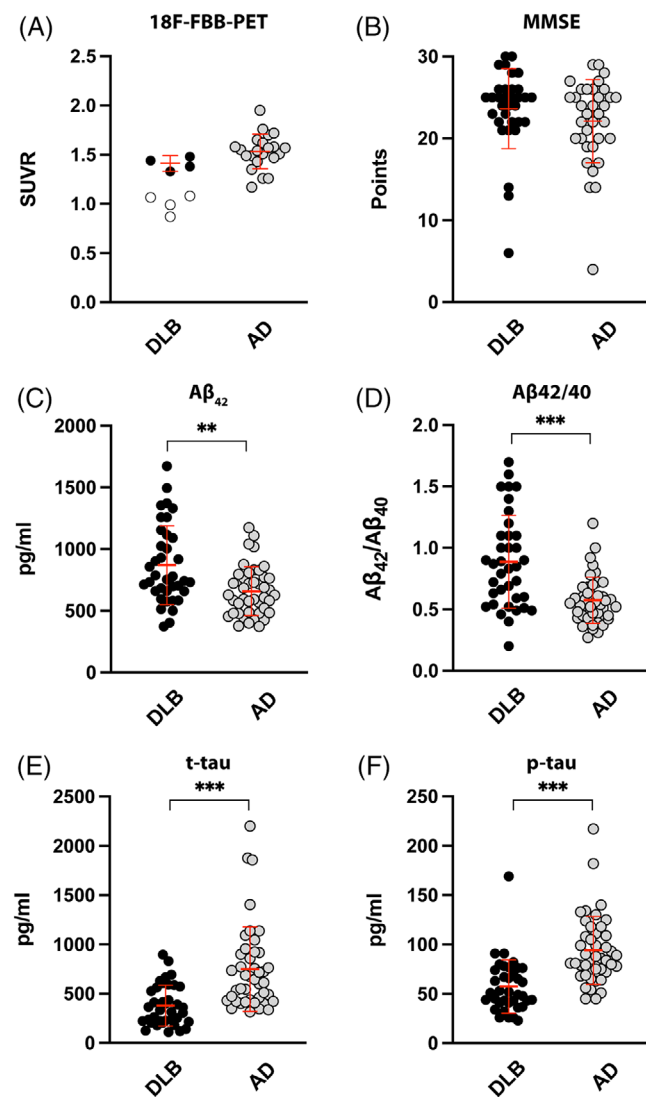
FIGURE 7 Additional biomarkers. (A) ^{18}F-FBB-PET results. Amyloid load in available ^{18}F-FBB-PET did not show significant differences between amyloid-positive DLB and AD patients. Open circles represent negative ^{18}F-FBB scans. (B) MMSE did not show significant differences between DLB and AD patients. (C-F) CSF biomarkers showed significant differences between DLB and AD patients. ANCOVA; **$p < .001$; ***$p < .0001$. ^{18}F-FBB, ^{18}F-Florbetaben; MMSE, Mini Mental State Examination; SUVR, standard uptake value ratio

^{18}F-Fluorodeoxyglucose-PET

Especially, ^{18}F-FDG-PET, which is a well-established in-vivo biomarker in the diagnosis of AD, showed an unsatisfying performance in the diagnosis of DLB so far and is "only" listed as a supportive biomarker in the McKeith criteria.[3]

^{18}F-FDG-PET is able to display patterns of cortical hypometabolism. DLB is characterized by a severe hypometabolism in occipital cortical areas that correlates with DLB neuropathology.[3,14] However, available data could not show satisfying diagnostic accuracies in differentiating DLB from AD. There are only few studies with larger sample sizes (>30

DLB patients) available showing diagnostic accuracies of visual PET assessment around 69%-72%,[6,15] which is consistent with our data.

Due to the pathological hallmarks of DLB with disproportional visuoperceptual impairments, occipital regions are strongly affected in DLB patients. Therefore, occipital hypometabolism is suggested as a key factor in the differential diagnosis between DLB and AD. However, diagnostic accuracy of ^{18}F-FDG-PET in the diagnosis of DLB and its differentiation to AD can be hampered due to overlapping cortical pathologies, especially between DLB and the AD variant of posterior cortical atrophy that also shows severe occipital involvement.

In order to improve the diagnostic accuracy, quantitative approaches with a more automated analysis that are less operator dependent are needed. Semiquantitative SPM-based analysis of ^{18}F-FDG-PET has previously shown to outperform the visual interpretation in discriminating between different types of dementia.[16,17]

In DLB diagnosis, higher performances could also be achieved by the addition of SPM-based analysis of occipital areas with better diagnostic accuracies of 78% up to 92%.[6,7,12,16,17] Caminiti et al.[12] showed the highest accuracy of 92% while using an optimized single-subject SPM analysis with comparison to a large database of normal controls using the presence of medial and lateral occipital hypometabolism to discriminate between DLB and AD. However, these results could not be reproduced in our current DLB cohort, even with the use of a comparable SPM-based analysis using statistical mapping of FDG uptake compared to a reliably cohort of normal patients. Combined lateral and medial occipital hypometabolism (above a –2 SD threshold compared to normal patients) could be detected in only 72% of DLB patients. In our semiquantitative analysis, the primary visual cortex showed the highest accuracy in differentiating DLB from AD patients with 77% for an optimal cutoff SUV of <1.348. Differences to Caminiti et al. might be explained by slightly different methodological approaches. However, our results were comparable to the other available studies.[6,7,12,16,17]

Cingulate island sign

A relative preservation of the posterior cingulate cortex in DLB patients was already described by Imamura et al. in 1997.[18] The visual assessment of the cingulate island sign showed a high specificity in several studies up to 100%, while it lacks sensitivity.[7,19] Results of our current study are in line with previous findings showing a specificity of the visual detection of the cingulate island sign of 93%-100% with a low sensitivity of 57%-62%. Furthermore, Le Gjerum et al.[20] emphasized a visual rating scale approach for the interpretation of the cingulate island sign yielding an accuracy of 72% in the differentiation of DLB from AD patients.

In order to improve diagnostic accuracy, the assessment of the cingulate island sign in a semiquantitative approach was further used. Lim et al.[7] first demonstrated the use of a cingulate island ratio in addition to visual ^{18}F-FDG-PET interpretation in DLB using a ratio of the posterior cingulate cortex to the precuneus and cuneus showing a diagnostic accuracy of 78%. Previous studies using the same ratio

showed comparable accuracies.[19,21] In our cohort, the ratio of the posterior cingulate cortex to the precuneus and cuneus showed a comparable accuracy of 77%.

In addition, we evaluated slightly different cingulate island ratios using cortical areas that represent the visual aspect of the cingulate island sign in order to examine whether another ratio is more suitable for the differentiation between DLB and AD. The ratio PCC/(VC+OCLAT) showed the best accuracy with 81%, even above the 80% threshold of a valid biomarker. This ratio including lateral occipital areas might better reflect occipital pathologies that occur in DLB leading to a clinically more relevant ratio. However, further prospective studies using this ratio should be performed in order to establish new ratios as indicative biomarkers in the diagnosis of DLB.

Interestingly, the uptake in the posterior cingulate region did not show significant differences between AD and DLB patients. These results are in line with previous findings of Whitwell et al.[19] and Lim et al.,[7] underlining that the posterior cingulate region alone is not appropriate to differentiate between DLB and AD. However, only the relative sparing of the posterior cingulate cortex metabolism reflected by the cingulate island sign appears as a valuable tool in the differential diagnosis of DLB.

Prodromal DLB and onset

In order to identify DLB patients as early as possible to provide early therapeutic interventions, a valid biomarker-based diagnosis is needed before the onset of fully developed DLB. Based on first occurring symptoms in a predementia stage, different prodromal DLB syndromes have been proposed by McKeith et al.[22] including MCI, delirium, psychiatric, and mixed onset.

However, the role of 18F-FDG-PET imaging in prodromal DLB stages remains unclear so far. In our study, we evaluated differences in 18F-FDG-PET between different onset types. While MCI- and psychiatric-onset groups did not show significant differences in cortical metabolism, mixed-onset patients showed a significantly lower 18F-FDG uptake in multiple cortical areas including the lateral prefrontal and lateral temporal cortex as well as the precuneus compared to MCI- or psychiatric-onset groups. This might be explained by a more severe pathology in patients with a mixed onset, or a mixed onset might represent a later stage of the disease. However, as we analyzed different onset types retrospectively based on clinical reports, our 18F-FDG-PET results do not precisely reflect the cerebral metabolism at the prodromal stage. The patient's clinical presentation after noticing first symptoms largely varied. Furthermore, decision on and when to perform a PET scan was made individually based on clinical decisions. Both issues lead to a heterogenous timepoint of performing the 18F-FDG-PET imaging. Therefore, a prospective study of the use of 18F-FDG-PET in patients presenting with different prodromal DLB symptoms as early as possible would be interesting for further evaluation of the predictive performance of PET imaging in prodromal DLB stages. Previous studies hinted on a hypometabolism in the primary visual cortex as a possible predictor of DLB in patients

with MCI onset.[23–25] However, other studies could not confirm those findings and even showed a significant amount of MCI patients with a typical AD pattern in 18F-FDG-PET converting to DLB.[26–28] Further studies on the potential use of 18F-FDG-PET in psychiatric or delirium onset are not available so far and should be in focus for future studies on prodromal dementia patients with possible prodromal DLB.

New quantitative approaches with strong cutoff definitions might help to improve the differentiation of DLB and AD in 18F-FDG-PET. Furthermore, the potential of 18F-FDG-PET imaging might be better fulfilled by the use of deep learning models in order to improve its diagnostic accuracy in the early diagnosis of DLB. A current study by Etmiami et al.[29] could already demonstrate a diagnostic accuracy for a 3-dimensional deep learning model for the detection of DLB of 96% using data from the Alzheimer's disease neuroimaging initiative and the European DLB Consortium.

Other biomarkers

In order to establish a valid biomarker-supported diagnosis of DLB, a combination of available biomarkers might be more suitable rather than one biomarker alone as different biomarkers represent different aspects of the complex disease comparable to AD biomarkers.[30]

While CSF biomarkers play an incremental role in the diagnosis of AD, their use in DLB remains unclear. Especially CSF Aß- and tau-biomarkers are more useful in the evaluation of AD pathologies. However, they can help to distinguish between DLB and AD. In our cohort, CSF tau biomarkers showed the highest accuracy in the differentiation between DLB and AD, which is in line with previous data.[31] A possibly more suitable CSF biomarker might be alpha-synuclein, while it is not clinically established yet due to controversial results in available studies.[32–35]

While 18F-FDG uptake correlated with t-tau in several brain regions, there was no correlation between 18F-FDG uptake and p-tau. Findings are in line with earlier studies of dementia patients that showed a strong association between t-tau and neuronal damage, while CSF phosphorylated tau proteins can lack this association and p-tau might be less sensitive as marker for neurofibrillary pathology.[36–38] Brain glucose metabolism is linked to neuronal dysfunction and neuron loss in the development of dementia and t-tau in CSF might better reflect neuronal damage compared to p-tau, which might explain these findings.

Furthermore, dopamine receptor imaging with 123I-FP-CIT is a well-established biomarker of DLB with high diagnostic accuracy distinguishing DLB from AD.[3] In our cohort, data were in line with previous studies (despite a limited number of AD cases with available 123I-FP-CIT imaging) with a diagnostic accuracy of 83%. There were no differences in the 123I-FP-CIT uptake between different onset groups. However, the diagnostic accuracy of 123I-FP-CIT scintigraphy in prodromal DLB was reported as low as 66% and even lower in MCI-DLB patients.[8]

A combination of 123I-FP-CIT and cardiac 123I-mIBG scintigraphy might be a suitable approach in order to improve diagnostic accuracy

to distinguish between DLB and other dementias as emphasized before.[39,40] Unfortunately, none of our studied patients underwent ^{123}I-mIBG scintigraphy. A major limitation of both ^{123}I-FP-CIT and cardiac ^{123}I-mIBG scintigraphy is the differentiation between DLB and other Parkinson's syndromes, an advantage of ^{18}F-FDG-PET imaging. Whether changes in brain metabolism precede changes in the noradrenergic and dopaminergic system (as Lewy body pathologies can spread starting at neocortical regions before substantia nigra involvement) should be further studied as well as possible differences between different DLB onset syndromes. Furthermore, ^{123}I-FP-CIT uptake did not correlate with ^{18}F-FDG nor ^{18}F-FBB uptake as pathologies reflect different aspects of the DLB pathology.

^{18}F-FBB-PET can be used in DLB as an in vivo biomarker of cerebral amyloid co-pathology. Earlier studies suggested that about 50% of DLB cases show a pathological amyloid load in ^{18}F-FBB-PET.[41] Cortical amyloid tracer binding has been shown to be able to distinguish between DLB and AD and even between DLB and mixed pathology with a significantly lower tracer uptake in DLB patients.[41] Furthermore, regional differences were described with relatively spared tracer uptake in the occipital lobes of DLB patients. In our study, 50% of available ^{18}F-FBB-PET scans of the DLB group showed a pathological ^{18}F-FBB uptake. However, ^{18}F-FBB uptake did not show significant differences between amyloid PET-positive DLB and the AD patients, neither in the whole brain region nor in different cortical regions, although in a limited number of available ^{18}F-FBB-PET data in our DLB group. ^{18}F-FBB uptake did not correlate with ^{18}F-FDG uptake in our cohort. ^{18}F-FBB-PET represents the distribution of extraneuronal amyloid plaques; however, the effect on neuronal destruction as measured by ^{18}F-FDG-PET remains unclear, especially in DLB patients. Earlier results showed that tau tangles, rather than amyloid plaques, better correlate with cognition and clinical symptoms in AD patients with regional patterns of amyloid deposition differing from tau deposition and atrophy patterns in autopsy findings.[42,43] Neuronal dysfunction seems to be the result of synergetic effects of tau and amyloid on predisposed neurons, while tau seems to be closely associated with neuronal deficits. However, more data on the interactions between amyloid load in ^{18}F-FBB-PET and ^{18}F-FDG uptake are needed, especially in DLB patients.

Limitations

A limitation of our study is the retrospective setting. Due to this study design, the data collection relied heavily on the patients' medical records and clinical examinations, without a standardized protocol for the use of different dementia biomarkers. As mentioned above, the time between the presence of first prodromal symptoms and the ^{18}F-FDG-PET highly varied between patients.

The use of clinical criteria in order to establish the diagnosis of DLB rather than histological proof, which was unavailable, might be the main limitation, thus the used clinical criteria and biomarkers have been validated before.

In order to overcome these limitations, prospective studies using ^{18}F-FDG-PET as early as possible after the appearance of first symptoms in larger cohorts are needed.

Overall, the optimal use of biomarkers in the diagnosis of DLB has not been found so far. However, both imaging and CSF biomarkers still show great potential for the use in suspected DLB patients. In our study, the highest diagnostic accuracy in the differentiation between DLB and AD was achieved by p-tau, 123I-FP-CIT scintigraphy, and the cingulate island ratio PCC/(VC+OCLAT). In order to predict the onset of DLB as early as possible, a bioinformatic modeling approach with the use of multiple biomarkers that represent different aspects of DLB pathology with respect to different DLB onset types might be a solution in the future. The cingulate island ratio has the potential to play a central role in future DLB diagnosis models next to new and established CSF or blood biomarkers, amyloid PET and clinical data, as well as results of neuropsychological tests. Models might provide specific networks for the differential diagnosis between DLB, AD, and other dementias with an optimal diagnostic performance. However, big data analysis on larger studies including more patients in a multicenter approach would be needed in order to create a suitable database for deep learning strategies.

ORCID

Caroline Bouter 🄳 https://orcid.org/0000-0002-0057-5037

REFERENCES

1. GBD 2019 Dementia Forecasting Collaborators. Estimation of the global prevalence of dementia in 2019 and forecasted prevalence in 2050: an analysis for the Global Burden of Disease Study 2019. Lancet Public Health. 2022;7:e105-e25.
2. Hogan DB, Fiest KM, Roberts JI, et al. The prevalence and incidence of dementia with Lewy bodies: a systematic review. Can J Neurol Sci. 2016;43(Suppl 1):S83-95.
3. McKeith IG, Boeve BF, Dickson DW, et al. Diagnosis and management of dementia with Lewy bodies: fourth consensus report of the DLB Consortium. Neurology. 2017;89:88-100.
4. Morenas-Rodriguez E, Sala I, Subirana A, et al. Clinical subtypes of dementia with Lewy bodies based on the initial clinical presentation. J Alzheimers Dis. 2018;64:505-13.
5. Foguem C, Manckoundia P. Lewy body disease: clinical and pathological "overlap syndrome" between synucleinopathies (Parkinson disease) and Tauopathies (Alzheimer disease). Curr Neurol Neurosci Rep. 2018;18:24.
6. O'Brien JT, Firbank MJ, Davison C, et al. 18F-FDG PET and perfusion SPECT in the diagnosis of Alzheimer and Lewy body dementias. J Nucl Med. 2014;55:1959-65.
7. Lim SM, Katsifis A, Villemagne VL, et al. The 18F-FDG PET cingulate island sign and comparison to 123I-beta-CIT SPECT for diagnosis of dementia with Lewy bodies. J Nucl Med. 2009;50:1638-45.
8. Thomas AJ, Donaghy P, Roberts G, et al. Diagnostic accuracy of dopaminergic imaging in prodromal dementia with Lewy bodies. Psychol Med. 2019;49:396-402.

9. Dubois B, Villain N, Frisoni GB, et al. Clinical diagnosis of Alzheimer's disease: recommendations of the International Working Group. Lancet Neurol. 2021;20:484-96.

10. Wabik A, Trypka E, Bladowska J, et al. Comparison of dynamic susceptibility contrast enhanced MR and FDG-PET brain studies in patients with Alzheimer's disease and amnestic mild cognitive impairment. J Transl Med. 2022;20:259.

11. Minoshima S, Frey KA, Koeppe RA, et al. A diagnostic approach in Alzheimer's disease using three-dimensional stereotactic surface projections of fluorine-18-FDG PET. J Nucl Med. 1995;36:1238-48.

12. Caminiti SP, Sala A, Iaccarino L, et al. Brain glucose metabolism in Lewy body dementia: implications for diagnostic criteria. Alzheimers Res Ther. 2019;11:20.

13. Mavroudis I, Petridis F, Kazis D. Cerebrospinal fluid, imaging, and physiological biomarkers in dementia with Lewy bodies. Am J Alzheimers Dis Other Demen. 2019;34:421-32.

14. Higuchi M, Tashiro M, Arai H, et al. Glucose hypometabolism and neuropathological correlates in brains of dementia with Lewy bodies. Exp Neurol. 2000;162:247-56.

15. Firbank MJ, Lloyd J, Williams D, et al. An evidence-based algorithm for the utility of FDG-PET for diagnosing Alzheimer's disease according to presence of medial temporal lobe atrophy. Br J Psychiatry. 2016;208:491-6.

16. Perani D, Della Rosa PA, Cerami C, et al. Validation of an optimized SPM procedure for FDG-PET in dementia diagnosis in a clinical setting. Neuroimage Clin. 2014;6:445-54.

17. Perani D, Cerami C, Caminiti SP, et al. Cross-validation of biomarkers for the early differential diagnosis and prognosis of dementia in a clinical setting. Eur J Nucl Med Mol Imaging. 2016;43:499-508.

18. Imamura T, Ishii K, Sasaki M, et al. Regional cerebral glucose metabolism in dementia with Lewy bodies and Alzheimer's disease: a comparative study using positron emission tomography. Neurosci Lett. 1997;235:49-52.

19. Whitwell JL, Graff-Radford J, Singh TD, et al. (18)F-FDG PET in posterior cortical atrophy and dementia with Lewy bodies. J Nucl Med. 2017;58:632-8.

20. Gjerum L, Frederiksen KS, Henriksen OM, et al. A visual rating scale for cingulate island sign on 18F-FDG-PET to differentiate dementia with Lewy bodies and Alzheimer's disease. J Neurol Sci. 2020;410:116645.

21. Graff-Radford J, Murray ME, Lowe VJ, et al. Dementia with Lewy bodies: basis of cingulate island sign. Neurology. 2014;83:801-9.

22. McKeith IG, Ferman TJ, Thomas AJ, et al. Research criteria for the diagnosis of prodromal dementia with Lewy bodies. Neurology. 2020;94:743-55.

23. Chiba Y, Iseki E, Fujishiro H, et al. Early differential diagnosis between Alzheimer's disease and dementia with Lewy bodies: comparison between (18)F-FDG PET and (123)I-IMP SPECT. Psychiatry Res Neuroimaging. 2016;249:105-12.

24. Fujishiro H, Iseki E, Kasanuki K, et al. A follow up study of non-demented patients with primary visual cortical hypometabolism: prodromal dementia with Lewy bodies. J Neurol Sci. 2013;334:48-54.

25. Fujishiro H, Iseki E, Kasanuki K, et al. Glucose hypometabolism in primary visual cortex is commonly associated with clinical features of dementia with Lewy bodies regardless of cognitive conditions. Int J Geriatr Psychiatry. 2012;27:1138-46.

26. Kondo D, Ota K, Kasanuki K, et al. Characteristics of mild cognitive impairment tending to convert into Alzheimer's disease or dementia with Lewy bodies: a follow-up study in a memory clinic. J Neurol Sci. 2016;369:102-8.

27. Clerici F, Del Sole A, Chiti A, et al. Differences in hippocampal metabolism between amnestic and non-amnestic MCI subjects: automated FDG-PET image analysis. Q J Nucl Med Mol Imaging. 2009;53:646-57.

28. Pardo JV, Lee JT, Kuskowski MA, et al. Fluorodeoxyglucose positron emission tomography of mild cognitive impairment with clinical follow-up at 3 years. Alzheimers Dement. 2010;6:326-33.

29. Etminani K, Soliman A, Davidsson A, et al. A 3D deep learning model to predict the diagnosis of dementia with Lewy bodies, Alzheimer's disease, and mild cognitive impairment using brain 18F-FDG PET. Eur J Nucl Med Mol Imaging. 2022;49:563-84.

30. Bouter C, Vogelgsang J, Wiltfang J. Comparison between amyloid-PET and CSF amyloid-beta biomarkers in a clinical cohort with memory deficits. Clin Chim Acta. 2019;492:62-8.

31. Bousiges O, Blanc F. Diagnostic value of cerebro-spinal fluid biomarkers in dementia with Lewy bodies. Clin Chim Acta. 2019;490:222-8.

32. Bousiges O, Bombois S, Schraen S, et al. Cerebrospinal fluid Alzheimer biomarkers can be useful for discriminating dementia with Lewy bodies from Alzheimer's disease at the prodromal stage. J Neurol Neurosurg Psychiatry. 2018;89:467-75.

33. Spies PE, Melis RJ, Sjogren MJ, et al. Cerebrospinal fluid alpha-synuclein does not discriminate between dementia disorders. J Alzheimers Dis. 2009;16:363-9.

34. Chiasserini D, Biscetti L, Eusebi P, et al. Differential role of CSF fatty acid binding protein 3, alpha-synuclein, and Alzheimer's disease core biomarkers in Lewy body disorders and Alzheimer's dementia. Alzheimers Res Ther. 2017;9:52.

35. Kapaki E, Paraskevas GP, Emmanouilidou E, et al. The diagnostic value of CSF alpha-synuclein in the differential diagnosis of dementia with Lewy bodies vs. normal subjects and patients with Alzheimer's disease. PLoS ONE. 2013;8:e81654.

36. Chiaravalloti A, Barbagallo G, Ricci M, et al. Brain metabolic correlates of CSF Tau protein in a large cohort of Alzheimer's disease patients: a CSF and FDG PET study. Brain Res. 2018;1678:116-22.

37. Buerger K, Alafuzoff I, Ewers M, et al. No correlation between CSF tau protein phosphorylated at threonine 181 with neocortical neurofibrillary pathology in Alzheimer's disease. Brain. 2007;130:e82.

38. Chiaravalloti A, Martorana A, Koch G, et al. Functional correlates of t-Tau, p-Tau and Abeta(1)(-)(4)(2) amyloid cerebrospinal fluid levels in Alzheimer's disease: a (1)(8)F-FDG PET/CT study. Nucl Med Commun. 2015;36:461-8.

39. Sakamoto F, Shiraishi S, Ogasawara K, et al. A diagnostic strategy for Lewy body disease using DAT-SPECT, MIBG and Combined index. Ann Nucl Med. 2020;34:415-23.

40. Kane JPM, Roberts G, Petrides GS, et al. (123)I-MIBG scintigraphy utility and cut-off value in a clinically representative dementia cohort. Parkinsonism Relat Disord. 2019;62:79-84.

41. Kantarci K, Lowe VJ, Chen Q, et al. beta-Amyloid PET and neuropathology in dementia with Lewy bodies. Neurology. 2020;94:e282-e91.

42. Rabinovici GD, Jagust WJ, Furst AJ, et al. Abeta amyloid and glucose metabolism in three variants of primary progressive aphasia. Ann Neurol. 2008;64:388-401.

43. Braak H, Braak E. Neuropathological stageing of Alzheimer-related changes. Acta Neuropathol. 1991;82:239-59.